Wireless Pers Commun
DOI 10.1007/s11277-012-0869-y

Time-Domain Block and Per-Tone Equalization for MIMO–OFDM in Shallow Underwater Acoustic Communication

Mojtaba Beheshti · Mohammad Javad Omidi · Ali Mohammad Doost-Hoseini

Abstract Shallow underwater acoustic (UWA) channel exhibits rapid temporal variations, extensive multipath spreads, and severe frequency-dependent attenuations. So, high data rate communication with high spectral efficiency in this challenging medium requires efficient system design. Multiple-input multiple-output orthogonal frequency-division multiplexing (MIMO–OFDM) is a promising solution for reliable transmission over highly dispersive channels. In this paper, we study the equalization of shallow UWA channels when a MIMO–OFDM transmission scheme is used. We address simultaneously the long multipath spread and rapid temporal variations of the channel. These features lead to interblock interference (IBI) along with intercarrier interference (ICI), thereby degrading the system performance. We describe the underwater channel using a general basis expansion model (BEM), and propose time-domain block equalization techniques to jointly eliminate the IBI and ICI. The block equalizers are derived based on minimum mean-square error and zero-forcing criteria. We also develop a novel approach to design two time-domain per-tone equalizers, which minimize bit error rate or mean-square error in each subcarrier. We simulate a typical shallow UWA channel to demonstrate the desirable performance of the proposed equalization techniques in Rayleigh and Rician fading channels.

Keywords Underwater acoustic channel · Multiple-input multiple-output (MIMO) · Orthogonal frequency division multiplexing (OFDM) · Basis expansion model (BEM) · Equalization

M. Beheshti (✉)
Information and Communication Technology Institute,
Isfahan University of Technology, Isfahan, Iran
e-mail: behesht@cc.iut.ac.ir

M. J. Omidi · A. M. Doost-Hoseini
Department of Electrical and Computer Engineering,
Isfahan University of Technology, Isfahan, Iran

Published online: 19 October 2012

1 Introduction

The interest in underwater acoustic (UWA) communications has grown steadily in the past three decades because of its applications in oceanography, marine commercial operations, underwater exploration, offshore oil industry and defense. Comprehensive research in these years has led to improved performance and reliability of UWA communication systems. Several review articles present an excellent overview of the progress made in this area [1,2]. The dominant features of the ocean environment that pose many challenges in designing robust UWA communication systems include limited bandwidth, time-varying (TV) multipath, severe fading and low velocity of acoustic propagation. UWA channels vary greatly depending on geometrical factors such as range, ocean depth, source/receiver depth, and environmental factors.

Shallow UWA communication channel is defined as a channel with large range-to-depth ratio. This channel is typically characterized by 1) a long delay spread resulting from the repeated sound reflections from the sea surface and floor, and 2) a high Doppler spread resulting from relative motion of the transmitter/receiver and movement of transducers, ocean surface, and internal waves. While most of the early high data rate experiments were reported for vertical links in deep water channels, shallow water horizontal communication has made significant progress only in the last decade.

Prior to 1990, UWA communication systems mainly relied on incoherent modulation and detection, such as M-ary frequency-shift keying (MFSK) [3]. However, the incoherent systems usually suffer from unnecessary, often substantial, bandwidth and power inefficiencies which makes them unsuitable for high-rate transmission. This forced the researchers to consider the use of coherent modulation. The first approach that demonstrated the feasibility of phase-coherent communication in horizontal shallow UWA channels was published in [4]. This approach employs the modulation schemes such as phase shift keying (PSK) along with decision feedback equalization and multichannel combining. However, the long multipath spread (of the order of 50 ms) and fast temporal variations of the shallow UWA channel often makes this method too complex for real-time applications.

As an alternative, orthogonal frequency division multiplexing (OFDM) has been studied for UWA communications. This is motivated by its successful applications in wireless communication over radio channels. In an OFDM system, the available bandwidth is divided into many subbands, so that the OFDM block duration is long compared to the multipath spread of the channel. Consequently, interblock interference (IBI) may be neglected in each subband. This considerably simplifies the complexity of channel equalization at the receiver. However, to have a suitable OFDM system for UWA applications, two issues must be addressed: 1) OFDM is sensitive to channel variations within a block which leads to intercarrier interference (ICI). UWA channels have rapid time variations due to the low speed of sound relative to the platform motion. Even in the absence of source/receiver motion, ICI could arise from surface/internal waves, internal turbulence and tidal flows. 2) OFDM uses a cyclic prefix (CP) larger than the maximum delay spread of the channel. The long delay spread encountered in UWA channels requires a long CP which decreases the bandwidth efficiency of the system. On the other hand, a short CP leads to IBI and ICI.

There have been several attempts to apply OFDM in UWA channels. In [5], the basic concepts and characteristics of the coded OFDM for UWA communications are described. Reference [6] presents the design criteria and analysis procedures of an OFDM system for broadband UWA communications. Frassati et al. [7] conduct a shallow water experiment to compare the performance of OFDM with direct sequence spread spectrum. A design of DFT-spread OFDM system applied to an UWA channel is presented in [8].

On the other hand, multi-input multi-output (MIMO) approaches have been recently applied to UWA communications [9,10]. MIMO is a general communication technique in which, multiple transmitting and receiving elements are used. This technique is utilized to exploit the multipath nature of UWA channel to provide diversity, multiplexing, or antenna gain, thereby improve the error performance, the bit rate, or the signal-to-interference-plus-noise ratio (SINR), respectively.

More recently, a MIMO extension to the OFDM scheme is also explored in the underwater context. In fact, MIMO and OFDM are parallel transmission schemes which exploit the space and frequency domain diversities, respectively, to improve the data rate and spectral efficiency. Li et al. [11] design a MIMO–OFDM system where null subcarriers are used for compensation of Doppler shifts and a maximum a posteriori (MAP) or zero-forcing (ZF) detector is used for MIMO demodulation. In [12] the performance of turbo-coded MIMO–OFDM systems with layered space time architectures in UWA channel is investigated. Reference [13] introduces a blind equalization approach for UWA MIMO–OFDM communication based on independent component analysis. In [14], frequency and time correlation of the underwater channel are exploited to obtain an adaptive channel estimation algorithm for MIMO–OFDM transmission.

The literature reviewed here, however, focuses mostly on the direct application of OFDM or MIMO–OFDM in UWA communications. In most of this literature, a CP much larger than the channel delay spread is used to avoid IBI. Using a long CP, decreases the spectral efficiency. Also, some of these efforts assume that the time variations of the channel within each OFDM block is slow enough to induce negligible ICI. On the other hand, the basic problem of equalization and interference cancellation for both single-input single-output (SISO)—and MIMO–OFDM transmission over wireless radio channels has been widely discussed. However, most of the works either discuss the impact of an insufficient CP [15] or the channel rapid time variations [16]. Therefore, most of the already proposed approaches for wireless radio channel cannot be directly applied in the context of underwater communications. These facts motivate us to propose a MIMO–OFDM scheme appropriate for the general class of UWA channels including shallow water channels, where both the ICI and IBI are present. In comparison to the existing literature, this paper focuses on the following aspects:

(i) We consider a shallow UWA channel that exhibits large delay spread and Doppler spread, simultaneously. We assume the CP is shorter than the channel delay spread and the channel varies within each OFDM block. Then, we employ a general basis expansion model (BEM) to approximate the UWA channel. The BEM coefficients, which are assumed to be known at the receiver are used to design the equalizer. BEM simplifies the equalizer design and reduces the complexity in channel estimation as the problem is reduced to estimating the basis coefficients.

(ii) We propose time-domain block minimum mean-square error (MMSE) and ZF equalizers for MIMO–OFDM transmission in shallow UWA channel to jointly mitigate the IBI and ICI.

(iii) We develop two time-domain per-tone equalizers which are based on bit error rate (BER) or mean-square error (MSE) minimization criteria. We note that all of the existing per-tone equalizers for OFDM, including our previous work [17], are frequency-domain approaches, whereas in this paper we suggest the idea of time-domain per-tone equalization.

(iv) We also show that our proposed time-domain per-tone equalizers are equivalent to the proposed block MMSE approach. In addition, the proposed approaches do not rely on a particular BEM for the UWA channel representation. Therefore, any BEM can be used.

Section 2 describes our system and data models. We derive time-domain block equalizers in Sect. 3. Time-domain per-tone equalization is introduced in Sect. 4. Section 5, discusses the complexity of the proposed approaches. In Sect. 6, we evaluate through computer simulations, the performance of the proposed equalizers. Finally, conclusions are drawn in Sect. 7.

Notation We use bold upper (lower) case letters to denote matrices (column vectors). $\mathcal{E}\{\cdot\}$ stands for the expectation and $\otimes$ represents the Kronecker product. $(\cdot)^*$, $(\cdot)^T$, and $(\cdot)^H$ represent conjugate, transpose, and Hermitian operators, respectively. We use $\mathrm{diag}\{\boldsymbol{x}\}$ to indicate a diagonal matrix with $\boldsymbol{x}$ as diagonal. $\boldsymbol{I}_m$ denotes the $m \times m$ identity matrix, and $\boldsymbol{0}_{m\times p}$ denotes the $m \times p$ all-zero matrix. Further, $\boldsymbol{\mathcal{F}}$ indicates the unitary fast Fourier transform (FFT) matrix; N is the FFT size; $\boldsymbol{\mathcal{F}}^{(k)}$ is the kth FFT matrix row; i is the OFDM block time index and T is the sampling time.

2 System and Data Models

Consider a MIMO–OFDM system with N_t transmit and N_r receive transducers shown in Fig. 1. We assume a simple spatial multiplexing scheme, in which the input data stream is partitioned into N_t parallel substreams and each substream is mapped into frequency-domain complex symbols and arranged into OFDM blocks of length N. Each block is then converted to the time domain by means of an N-point inverse fast Fourier transform (IFFT) and extended with a CP of length c. The time-domain blocks of parallel substreams are then transmitted in UWA channel by N_t transmit transducers. At the receiver, time-domain equalization along with FFT demodulation is performed to detect the transmitted symbols. Let $x_k^{(t)}[i]$ be the quadrature amplitude modulation (QAM) symbol transmitted on the kth subcarrier of the ith OFDM block in the tth substream. The QAM symbols are assumed to be independent and identically distributed (i.i.d) random variables with equal variance σ_s^2. The time-domain sequence $u^{(t)}[n]$ transmitted from the tth transducer is given by

$$u^{(t)}[n] = \frac{1}{\sqrt{N}} \sum_{k=0}^{N-1} x_k^{(t)}[i] e^{j2\pi \bar{n} k/N} \tag{1}$$

where $i = \lfloor n/(N+c) \rfloor$, and $\bar{n} = n - i(N+c) - c$.

The acoustic channel characterizing the link between the tth transmit transducer and the rth receive transducer at time-index n and discrete time-delay θ is denoted by $g^{(r,t)}[n;\,\theta]$. We assume that there is sufficient spacing between the transmit (receive) transducers

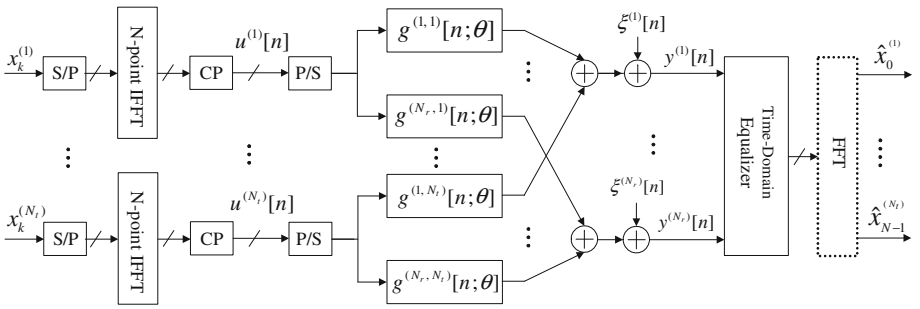

Fig. 1 MIMO–OFDM system model

relative to the channel coherence distance to ensure statistically independent channels for each transmitter-receiver pair. Using the baseband description, we express the received sample sequence at the rth receive transducer at time-index n, $y^{(r)}[n]$ as

$$y^{(r)}[n] = \sum_{t=1}^{N_t} \sum_{\theta=0}^{+\infty} g^{(r,\,t)}[n;\ \theta] u^{(t)}[n-\theta] + \xi^{(r)}[n] \tag{2}$$

where $\xi^{(r)}[n]$ is the zero-mean complex Gaussian noise at the rth receive transducer. We assume that the noise is independent of the transmitted sequence.

We use BEM to describe the UWA channel $g^{(r,\,t)}[n;\theta]$. In BEM, the TV channel $g^{(r,\,t)}[n;\theta]$ is modeled as a TV finite impulse response (FIR) filter $h^{(r,\,t)}[n;\theta]$ of order $L = \lfloor \tau_{\max}/T \rfloor + 1$, where $\tau_{\max}$ is the maximum delay spread of the UWA channel, and each tap is approximated as the weighted sum of a few basis functions. Using BEM, we can express the lth tap of the TV FIR channel between the tth transmit transducer and the rth receive transducer for $n \in \{\, i(N+c)+c+d-L'+1,\ \ldots,\ (i+1)(N+c)+d \,\}$ as

$$h^{(r,\,t)}[n;\,l] = \sum_{q=-Q/2}^{Q/2} h_{q,l}^{(r,\,t)} \psi_q[n] \tag{3}$$

where d is some synchronization (decision) delay, L' is a constant greater than or equal to the channel order L, $\left\{h_{q,l}^{(r,\,t)}\right\}$ are the BEM coefficients and $\left\{\psi_q[n]\right\}$ are the basis functions. The BEM coefficients remain invariant over a period of length $(N+L')T$.

Recently, BEMs have been widely used as a feasible representation of doubly selective channels [18–21]. Different BEMs have different basis functions. In the discrete prolate spheroidal BEM (DPS-BEM), the basis functions are the most significant eigenvectors of a kernel matrix [18]. Polynomial BEM (P-BEM) uses a set of polynomial functions [19], and the discrete Karhunen-Loveve BEM (DKL-BEM) uses the eigenvectors corresponding to the largest eigenvalues of the channel covariance matrix [20]. Finally, in complex exponential BEM (CE-BEM), basis functions are complex exponential (Fourier) functions [21]. In this study, we use a general BEM as in (3) to characterize the underwater channel and design the proposed equalizers. So, our formulation is general and can be applied using different BEMs.

We substitute the BEM channel model in (2) to write the received sample sequence at the rth receive transducer, for $n \in \left\{i(N+c)+c+d-L'+1,\ldots,\ (i+1)(N+c)+d\right\}$ as

$$y^{(r)}[n] = \sum_{t=1}^{N_t} \sum_{q=-Q/2}^{Q/2} \sum_{l=0}^{L} h_{q,l}^{(r,\,t)} \psi_q[n] u^{(t)}[n-l] + \xi^{(r)}[n] \tag{4}$$

The Eq. (4) is an approximation of the relation in (2) and is used only to simplify the design of the proposed equalizers, deployed in the actual channel. Here we use a matrix representation to express the received block of length $N+L'$ at the rth receive transducer as

$$\begin{aligned} \boldsymbol{y}^{(r)}[i] &= \sum_{t=1}^{N_t} \underbrace{\sum_{q=-Q/2}^{Q/2} \boldsymbol{\Psi}_q[i] \left[\boldsymbol{O}_1,\, \boldsymbol{H}_q^{(r,\,t)}[i],\, \boldsymbol{O}_2\right] (\boldsymbol{I}_3 \otimes \boldsymbol{P})(\boldsymbol{I}_3 \otimes \boldsymbol{\mathcal{F}}^H)}_{\boldsymbol{G}^{(r,\,t)}[i]} \underbrace{\begin{bmatrix} \boldsymbol{x}^{(t)}[i-1] \\ \boldsymbol{x}^{(t)}[i] \\ \boldsymbol{x}^{(t)}[i+1] \end{bmatrix}}_{\tilde{\boldsymbol{x}}^{(t)}} + \boldsymbol{\xi}^{(r)}[i] \\ &= \sum_{t=1}^{N_t} \boldsymbol{G}^{(r,\,t)}[i] \tilde{\boldsymbol{x}}^{(t)} + \boldsymbol{\xi}^{(r)}[i] = \boldsymbol{G}_T^{(r)}[i] \tilde{\boldsymbol{x}} + \boldsymbol{\xi}^{(r)}[i] \end{aligned} \tag{5}$$

where i is the block index, $\boldsymbol{y}^{(r)}[i] = [y^{(r)}[i(N+c)+c+d-L'+1], \ldots, y^{(r)}[(i+1)(N+c) + d]]^T$, $\boldsymbol{\Psi}_q[i] = \text{diag}\{[\psi_q[i(N+c)+c+d-L'+1], \ldots, \psi_q](i+1)(N+c)+d]]\}$, $\boldsymbol{O}_1 = \boldsymbol{0}_{(N+L')\times(N+2c+d-L-L')}$, $\boldsymbol{O}_2 = \boldsymbol{0}_{(N+L')\times(N+c-d)}$, $\boldsymbol{H}_q^{(r,t)}[i]$ is an $(N+L')\times(N+L+L')$ Toeplitz matrix with the first column $[h_{q,L}^{(r,t)}[i], \boldsymbol{0}_{1\times(N+L'-1)}]^T$ and the first row $[h_{q,L}^{(r,t)}[i], \ldots, h_{q,0}^{(r,t)}[i], \boldsymbol{0}_{1\times(N+L'-1)}]$, $\boldsymbol{x}^{(t)}[i] = [x_0^{(t)}[i], \ldots, x_{N-1}^{(t)}[i]]^T$, $\boldsymbol{\xi}^{(r)}[i] = [\xi^{(r)}[i(N+c)+c+d-L'+1], \ldots, \xi^{(r)}[(i+1)(N+c)+d]]^T$, $\boldsymbol{G}_T^{(r)}[i] = [\boldsymbol{G}^{(r,1)}[i], \ldots, \boldsymbol{G}^{(r,N_t)}[i]]$, $\tilde{\boldsymbol{x}} = [\tilde{\boldsymbol{x}}^{(1)\,T}, \ldots, \tilde{\boldsymbol{x}}^{(N_t)\,T}]^T$ and $\boldsymbol{P}$ is the CP insertion matrix given by

$$\boldsymbol{P} = \begin{bmatrix} \boldsymbol{0}_{c\times(N-c)} & \boldsymbol{I}_c \\ & \boldsymbol{I}_N \end{bmatrix}$$

The data model in (5) is an extension of Eq. (10) in [22] to the MIMO–OFDM case with the general BEM of (3). To derive this model, we assume that three successive blocks with indices $i-1$, i and $i+1$ are transmitted. The ith block is of interest and the previous and the following blocks are used to include the IBI from neighboring blocks in our model. Using (5) and defining $\boldsymbol{y}[i] = [\boldsymbol{y}^{(1)\,T}[i], \ldots, \boldsymbol{y}^{(N_r)\,T}[i]]^T$, $\boldsymbol{G}[i] = [\boldsymbol{G}_T^{(1)\,T}[i], \ldots, \boldsymbol{G}_T^{(N_r)\,T}[i]]^T$ and $\boldsymbol{\xi}[i] = [\boldsymbol{\xi}^{(1)\,T}[i], \ldots, \boldsymbol{\xi}^{(N_r)\,T}[i]]^T$, we can write the received blocks (each of length $N+L'$) at all receive transducers as

$$\boldsymbol{y}[i] = \boldsymbol{G}[i]\tilde{\boldsymbol{x}} + \boldsymbol{\xi}[i] \tag{6}$$

3 Time-Domain Block Equalization

In this section, we address time-domain block equalization to simultaneously mitigate IBI and ICI for communication in the shallow UWA channel. We consider MIMO–OFDM transmission and focus on the MMSE and ZF equalizers. At the receiver, we apply a bank of N_t time-varying (TV) filters (equalizers) at each receive transducer (Fig. 2). The outputs of the corresponding filters are combined and passed through the FFT-demodulator to recover the transmitted blocks on different transmit transducers. In this sense, the TV filters $\boldsymbol{G}_e^{(r,a)}[i]$

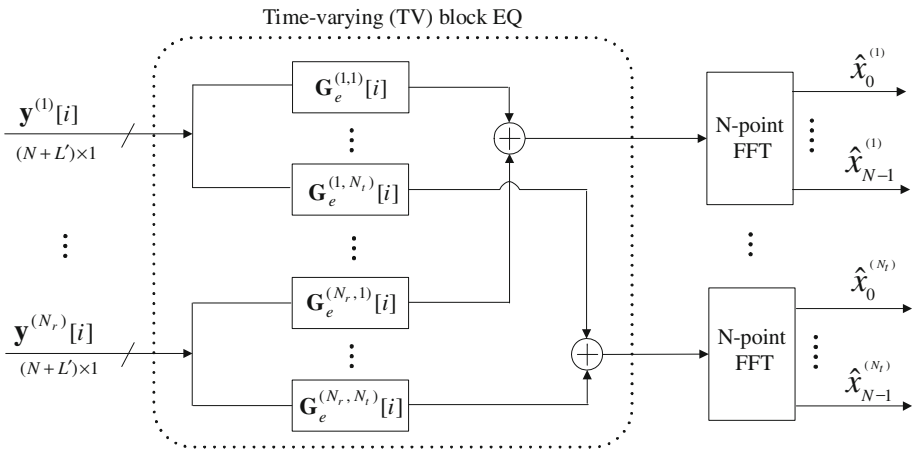

Fig. 2 Proposed time-domain block MMSE equalizer

for $r = 1, \ldots, N_r$ are designed and applied at the receive transducers to recover the transmitted block on the ath transmit transducer for $a = 1, \ldots, N_t$. Hence, we estimate the ith transmitted block on the ath transmit transducer as

$$\hat{\boldsymbol{x}}^{(a)}[i] = \mathcal{F}\left(\sum_{r=1}^{N_r} \boldsymbol{G}_e^{(r,\,a)}[i]\boldsymbol{y}^{(r)}[i]\right) \tag{7}$$

Defining $\boldsymbol{x}[i] = [\boldsymbol{x}^{(1)\,T}[i], \ldots, \boldsymbol{x}^{(N_t)\,T}[i]]^T$, $\boldsymbol{G}_e^{(a)}[i] = [\boldsymbol{G}_e^{(1,\,a)}[i], \ldots, \boldsymbol{G}_e^{(N_r,\,a)}[i]]$ and $\boldsymbol{G}_e[i] = [\boldsymbol{G}_e^{(1)\,T}[i], \ldots, \boldsymbol{G}_e^{(N_t)\,T}[i]]^T$, and considering the transmitted blocks on all transmit transducers, we can extend (7) to obtain an estimate of $\boldsymbol{x}[i]$ as

$$\hat{\boldsymbol{x}}[i] = (\boldsymbol{I}_{N_t} \otimes \mathcal{F})\boldsymbol{G}_e[i]\boldsymbol{y}[i] \tag{8}$$

Time-domain MMSE equalization amounts to finding the block equalizer $\boldsymbol{G}_e[i]$ such that $\hat{\boldsymbol{x}}[i]$ is closest to $\boldsymbol{x}[i]$ in the MMSE sense, i.e.

$$\boldsymbol{G}_{e,\,\mathrm{MMSE}}[i] = \arg\min_{\boldsymbol{G}_e[i]} \mathcal{E}\left\{\left\|\boldsymbol{x}[i] - (\boldsymbol{I}_{N_t} \otimes \mathcal{F})\boldsymbol{G}_e[i]\boldsymbol{y}[i]\right\|^2\right\} \tag{9}$$

At this point, we express the received sample sequence $\boldsymbol{y}[i]$ in another form to explicitly include $\boldsymbol{x}[i]$. In (5), $\tilde{\boldsymbol{x}}^{(t)}$ can be written as a linear combination of the ith, $(i-1)$st, and $(i+1)$st transmitted blocks on the tth transmit transducer as

$$\tilde{\boldsymbol{x}}^{(t)} = \boldsymbol{E}_{-1}\boldsymbol{x}^{(t)}[i-1] + \boldsymbol{E}_0\boldsymbol{x}^{(t)}[i] + \boldsymbol{E}_1\boldsymbol{x}^{(t)}[i+1] \tag{10}$$

where $\boldsymbol{E}_{-1} = [\boldsymbol{I}_N, \boldsymbol{0}_{N\times N}, \boldsymbol{0}_{N\times N}]^T$, $\boldsymbol{E}_0 = [\boldsymbol{0}_{N\times N}, \boldsymbol{I}_N, \boldsymbol{0}_{N\times N}]^T$, and $\boldsymbol{E}_1 = [\boldsymbol{0}_{N\times N}, \boldsymbol{0}_{N\times N}, \boldsymbol{I}_N]^T$. We can extend (10) to include the transmitted blocks on all transmit transducers as follows:

$$\begin{aligned}\tilde{\boldsymbol{x}} = \begin{bmatrix}\tilde{\boldsymbol{x}}^{(1)}\\ \vdots \\ \tilde{\boldsymbol{x}}^{(N_t)}\end{bmatrix} &= \underbrace{(\boldsymbol{I}_{N_t} \otimes \boldsymbol{E}_{-1})}_{\mathbb{E}_{-1}}\begin{bmatrix}\boldsymbol{x}^{(1)}[i-1]\\ \vdots \\ \boldsymbol{x}^{(N_t)}[i-1]\end{bmatrix} + \underbrace{(\boldsymbol{I}_{N_t} \otimes \boldsymbol{E}_0)}_{\mathbb{E}_0}\begin{bmatrix}\boldsymbol{x}^{(1)}[i]\\ \vdots \\ \boldsymbol{x}^{(N_t)}[i]\end{bmatrix}\\ &+ \underbrace{(\boldsymbol{I}_{N_t} \otimes \boldsymbol{E}_1)}_{\mathbb{E}_1}\begin{bmatrix}\boldsymbol{x}^{(1)}[i+1]\\ \vdots \\ \boldsymbol{x}^{(N_t)}[i+1]\end{bmatrix} = \mathbb{E}_{-1}\boldsymbol{x}[i-1] + \mathbb{E}_0\boldsymbol{x}[i] + \mathbb{E}_1\boldsymbol{x}[i+1]\end{aligned} \tag{11}$$

Substituting (11) in (6) and using the definition $\boldsymbol{v}[i] = \boldsymbol{G}[i]\mathbb{E}_{-1}\boldsymbol{x}[i-1] + \boldsymbol{G}[i]\mathbb{E}_1\boldsymbol{x}[i+1] + \boldsymbol{\xi}[i]$, we obtain

$$\boldsymbol{y}[i] = \boldsymbol{G}[i]\mathbb{E}_0\boldsymbol{x}[i] + \boldsymbol{v}[i] \tag{12}$$

Using (12), the solution of minimization problem in (9) is given by [23]

$$\boldsymbol{G}_{e,\,\mathrm{MMSE}}[i] = (\boldsymbol{I}_{N_t} \otimes \mathcal{F}^H)\boldsymbol{R}_x(\boldsymbol{G}[i]\mathbb{E}_0)^H\left(\boldsymbol{G}[i]\mathbb{E}_0\boldsymbol{R}_x(\boldsymbol{G}[i]\mathbb{E}_0)^H + \boldsymbol{R}_v\right)^{-1} \tag{13a}$$

$$= (\boldsymbol{I}_{N_t} \otimes \mathcal{F}^H)\left((\boldsymbol{G}[i]\mathbb{E}_0)^H\boldsymbol{R}_v^{-1}\boldsymbol{G}[i]\mathbb{E}_0 + \boldsymbol{R}_x^{-1}\right)^{-1}(\boldsymbol{G}[i]\mathbb{E}_0)^H\boldsymbol{R}_v^{-1} \tag{13b}$$

where

$$\begin{aligned}\boldsymbol{R}_v &= \mathcal{E}\left\{\boldsymbol{v}[i]\boldsymbol{v}^H[i]\right\} = \boldsymbol{G}[i](\mathbb{E}_{-1}\boldsymbol{R}_x\mathbb{E}_{-1}^H + \mathbb{E}_1\boldsymbol{R}_x\mathbb{E}_1^H)\boldsymbol{G}^H[i] + \boldsymbol{R}_\xi,\\ \boldsymbol{R}_x &= \mathcal{E}\left\{\boldsymbol{x}[i]\boldsymbol{x}^H[i]\right\},\ \boldsymbol{R}_\xi = \mathcal{E}\left\{\boldsymbol{\xi}[i]\boldsymbol{\xi}^H[i]\right\}\end{aligned} \tag{14}$$

Note that (13b) is obtained from (13a) by applying the matrix inversion lemma. For white input data and noise with variances σ_s^2 and σ_ξ^2, respectively ($\boldsymbol{R}_x = \sigma_s^2 \boldsymbol{I}_{(N_t N)}$, $\boldsymbol{R}_\xi = \sigma_\xi^2 \boldsymbol{I}_{N_r(N+L')}$), the MMSE equalizer reduces to

$$\boldsymbol{G}_{e,\,\mathrm{MMSE}}[i] = (\boldsymbol{I}_{N_t} \otimes \boldsymbol{\mathcal{F}}^H)\mathbb{E}_0{}^H \left(\boldsymbol{G}^H[i]\boldsymbol{G}[i] + \frac{\sigma_\xi^2}{\sigma_s^2} \boldsymbol{I}_{(3NN_t)} \right)^{-1} \boldsymbol{G}^H[i] \tag{15}$$

We can obtain the ZF solution by setting the signal power to infinity in the MMSE solution (13b). Hence the ZF equalizer is obtained as

$$\boldsymbol{G}_{e,\,\mathrm{ZF}}[i] = (\boldsymbol{I}_{N_t} \otimes \boldsymbol{\mathcal{F}}^H) \left((\boldsymbol{G}[i]\mathbb{E}_0)^H \boldsymbol{R}_v^{-1} \boldsymbol{G}[i]\mathbb{E}_0 \right)^{-1} (\boldsymbol{G}[i]\mathbb{E}_0)^H \boldsymbol{R}_v^{-1} \tag{16}$$

The existence of the ZF solution requires that the matrix $\boldsymbol{G}[i]\mathbb{E}_0$ has full column rank. A necessary condition for $\boldsymbol{G}[i]\mathbb{E}_0$ to have full column rank is that the inequality $N_r(N + L') \geq N_t N$ is satisfied. For sufficiently large N, this inequality is satisfied when the number of receive transducers is larger than or equal to the number of transmit transducers, i.e. $N_r \geq N_t$. Note that the MMSE solution always exists regardless of the number of receive transducers. However, it is evident that the performance of the MMSE equalizer will improve if it is designed in such a way that the corresponding ZF equalizer exist.

4 Time-Domain Per-Tone Equalization

In Sect. 3, we derived a time-domain block MMSE equalizer to combat the effect of the UWA propagation channel. This equalizer estimates the transmitted blocks on all transmit transducers as

$$\hat{\boldsymbol{x}}[i] = (\boldsymbol{I}_{N_t} \otimes \boldsymbol{\mathcal{F}})\boldsymbol{G}_{e,\,\mathrm{MMSE}}[i]\boldsymbol{y}[i] \triangleq \bar{\boldsymbol{G}}_{e,\,\mathrm{MMSE}}[i]\boldsymbol{y}[i] \tag{17}$$

Equation (17) shows that the transmitted QAM symbol on each subcarrier can be estimated using a linear combination of the received data samples of all receive transducers. Here, we use this fact to propose two time-domain per-tone equalization methods based on BER and MSE minimization, respectively.

4.1 BER Minimization Method

In this subsection, we first introduce a BER model and then, develop the equalization method. Consider an M-QAM system with a square constellation of size $M = 2^{2m}$ for some integer m. This system can be viewed as two $\sqrt{M}$-pulse amplitude modulation (PAM) systems in quadrature. The probability of symbol error for each $\sqrt{M}$-PAM system is [24]

$$\mathcal{P}_{\sqrt{M}} = 2\left(1 - \frac{1}{\sqrt{M}}\right) Q\left(\sqrt{\frac{6}{M-1}\frac{\gamma_s}{2}}\right) \tag{18}$$

where γ_s is the average signal-to-noise ratio (SNR) of the M-QAM system and the Q-function is defined as $Q(x) = (1/\sqrt{2\pi}) \int_x^\infty exp\,(-x^2/2)\,dx\,,\ x \geq 0$. In this study, we consider 4-QAM signaling and assume that the residual interference and noise at the output of each subcarrier has Gaussian distribution. So, the BER for the kth subcarrier of the ith OFDM block corresponding to the ath transmit transducer is obtained from (18) by substituting $M = 4$ and $\gamma_s = \mathrm{SINR}^{(a,k)}[i]$, which yields

$$\mathcal{P}_{\text{bit}}^{(a,k)}[i] = Q\left(\sqrt{\text{SINR}^{(a,k)}[i]}\right) \tag{19}$$

where $\text{SINR}^{(a,k)}[i]$ is the average SINR on subcarrier k of the ith OFDM block for the ath transmit transducer. Finally, we average the subcarrier BER (19) over used subcarriers to get the total BER corresponding to the ith OFDM block and the ath transmit transducer as

$$\mathcal{P}_{\text{bit}}^{(a)}[i] = \frac{1}{N_u} \sum_{k \in \mathcal{S}_u} Q\left(\sqrt{\text{SINR}^{(a,k)}[i]}\right) \tag{20}$$

where $\mathcal{S}_u$ is the set of used subcarriers with N_u elements.

We now develop a per-tone equalization method which minimizes the total BER in (20). To estimate the transmitted symbol on the kth subcarrier of the ith OFDM block at the ath transmit transducer, we can use the following linear combination in the time domain:

$$\hat{x}_k^{(a)}[i] = \sum_{r=1}^{N_r} \boldsymbol{w}^{(r,a,k)\,T}[i]\boldsymbol{y}^{(r)}[i] \tag{21}$$

where $\boldsymbol{w}^{(r,a,k)}[i] = [w_0^{(r,a,k)}[i], \ldots, w_{N+L'-1}^{(r,a,k)}[i]]^T$. Using (5) and (10), we can rewrite (21) as

$$\begin{aligned}
\hat{x}_k^{(a)}[i] = &\sum_{r=1}^{N_r} \boldsymbol{w}^{(r,a,k)T}[i]\boldsymbol{G}^{(r,a)}[i]\boldsymbol{E}_0\boldsymbol{x}^{(a)}[i] \\
&+ \sum_{r=1}^{N_r} \boldsymbol{w}^{(r,a,k)T}[i]\boldsymbol{G}^{(r,a)}[i]\boldsymbol{E}_{-1}\boldsymbol{x}^{(a)}[i-1] \\
&+ \sum_{r=1}^{N_r} \boldsymbol{w}^{(r,a,k)\,T}[i]\boldsymbol{G}^{(r,a)}[i]\boldsymbol{E}_1\boldsymbol{x}^{(a)}[i+1] \\
&+ \sum_{r=1}^{N_r} \boldsymbol{w}^{(r,a,k)\,T}[i] \sum_{\substack{t=1 \\ t\neq a}}^{N_t} \boldsymbol{G}^{(r,t)}[i]\tilde{\boldsymbol{x}}^{(t)} \\
&+ \sum_{r=1}^{N_r} \boldsymbol{w}^{(r,a,k)\,T}[i]\boldsymbol{\xi}^{(r)}[i]
\end{aligned} \tag{22}$$

Defining $\boldsymbol{w}^{(a,k)}[i] = [\boldsymbol{w}^{(1,a,k)\,T}[i], \ldots, \boldsymbol{w}^{(N_r,a,k)\,T}[i]]^H$ and $\boldsymbol{G}_R^{(a)}[i] = [\boldsymbol{G}^{(1,a)\,T}[i], \ldots, \boldsymbol{G}^{(N_r,a)\,T}[i]]^T$, we express (22) as

$$\begin{aligned}
\hat{x}_k^{(a)}[i] = &\underbrace{\boldsymbol{w}^{(a,k)H}[i]\boldsymbol{G}_R^{(a)}[i]\boldsymbol{E}_0}_{\boldsymbol{b}_1^H[i]}\boldsymbol{x}^{(a)}[i] + \underbrace{\boldsymbol{w}^{(a,k)H}[i]\boldsymbol{G}_R^{(a)}[i]\boldsymbol{E}_{-1}}_{\boldsymbol{b}_2^H[i]}\boldsymbol{x}^{(a)}[i-1] \\
&+ \underbrace{\boldsymbol{w}^{(a,k)H}[i]\boldsymbol{G}_R^{(a)}[i]\boldsymbol{E}_1}_{\boldsymbol{b}_3^H[i]}\boldsymbol{x}^{(a)}[i+1] + \underbrace{\sum_{r=1}^{N_r} \boldsymbol{w}^{(r,a,k)\,T}[i] \sum_{\substack{t=1 \\ t\neq a}}^{N_t} \boldsymbol{G}^{(r,t)}[i]\tilde{\boldsymbol{x}}^{(t)}}_{\boldsymbol{w}^{(a,k)H}[i]\boldsymbol{b}_4[i]} \\
&+ \boldsymbol{w}^{(a,k)H}[i]\boldsymbol{\xi}[i]
\end{aligned} \tag{23}$$

Or equivalently

$$\hat{x}_k^{(a)}[i] = b_{1,k}^*[i]x_k^{(a)}[i] + \sum_{\substack{m=0 \\ m\neq k}}^{N-1} b_{1,m}^*[i]x_m^{(a)}[i] + \sum_{m=0}^{N-1} b_{2,m}^*[i]x_m^{(a)}[i-1] + \sum_{m=0}^{N-1} b_{3,m}^*[i]x_m^{(a)}[i+1] + \boldsymbol{w}^{(a,k)H}[i]\boldsymbol{b}_4[i] + \boldsymbol{w}^{(a,k)H}[i]\boldsymbol{\xi}[i] \quad (24)$$

where $b_{J,m}[i]$ and $x_m^{(a)}[i]$ are the $(m+1)$th elements of vectors $\boldsymbol{b}_J[i]$ and $\boldsymbol{x}^{(a)}[i]$, respectively.

The first term in (24) contains the desired signal component and the second is the ICI component. The third and fourth terms are IBI contributions from the previous and the following blocks, respectively. The fifth term is interference from other transmit transducers or inter-transducer interference (ITI), and the last term is additive noise. We define the SINR for the kth frequency bin of the ith OFDM block and the ath transmit transducer as

$$\mathrm{SINR}^{(a,k)}[i] = P_s^{(a,k)}[i]/(P_{\mathrm{ICI}}^{(a,k)}[i] + P_{\mathrm{IBI}_p}^{(a,k)}[i] + P_{\mathrm{IBI}_f}^{(a,k)}[i] + P_{\mathrm{ITI}}^{(a,k)}[i] + P_{\mathrm{noise}}^{(a,k)}[i]) \quad (25)$$

where $P_s^{(a,k)}[i]$ denotes the signal power and $P_{\mathrm{ICI}}^{(a,k)}[i]$ is the ICI power. $P_{\mathrm{IBI}_p}^{(a,k)}[i]$ and $P_{\mathrm{IBI}_f}^{(a,k)}[i]$ represent the IBI powers due to the previous and the following blocks, respectively. $P_{\mathrm{ITI}}^{(a,k)}[i]$ denotes the interference power caused by other transmit transducers and $P_{\mathrm{noise}}^{(a,k)}[i]$ is the noise power. Considering white input data and noise, we derive the power terms as follows:

$$\begin{aligned}
P_s^{(a,k)}[i] &= \mathcal{E}\left\{\left|x_k^{(a)}[i]\right|^2\right\}\mathcal{E}\left\{\left|b_{1,k}^*[i]\right|^2\right\} = \sigma_s^2\left|\boldsymbol{b}_1^H[i]\boldsymbol{e}^{(k)}\right|^2 \\
&= \sigma_s^2\boldsymbol{w}^{(a,k)H}[i]\boldsymbol{w}_k^{(a)}[i]\boldsymbol{w}_k^{(a)H}[i]\boldsymbol{w}^{(a,k)}[i] \\
P_{\mathrm{ICI}}^{(a,k)}[i] &= \sum_{\substack{m=0 \\ m\neq k}}^{N-1}\mathcal{E}\left\{\left|b_{1,m}^*[i]x_m^{(a)}[i]\right|^2\right\} = \sigma_s^2\sum_{\substack{m=0 \\ m\neq k}}^{N-1}\left|\boldsymbol{b}_1^H[i]\boldsymbol{e}^{(m)}\right|^2 \\
&= \sigma_s^2\boldsymbol{w}^{(a,k)H}[i]\boldsymbol{G}_R^{(a)}[i]\boldsymbol{E}_0\left(\boldsymbol{I}_N - \boldsymbol{e}^{(k)}\boldsymbol{e}^{(k)T}\right)\boldsymbol{E}_0^H\boldsymbol{G}_R^{(a)H}[i]\boldsymbol{w}^{(a,k)}[i] \\
P_{\mathrm{IBI}_p}^{(a,k)}[i] &= \sigma_s^2\sum_{m=0}^{N-1}\left|\boldsymbol{b}_2^H[i]\boldsymbol{e}^{(m)}\right|^2 = \sigma_s^2\boldsymbol{w}^{(a,k)H}[i]\boldsymbol{G}_R^{(a)}[i]\boldsymbol{E}_{-1}\boldsymbol{E}_{-1}^H\boldsymbol{G}_R^{(a)H}[i]\boldsymbol{w}^{(a,k)}[i] \\
P_{\mathrm{IBI}_f}^{(a,k)}[i] &= \sigma_s^2\sum_{m=0}^{N-1}\left|\boldsymbol{b}_3^H[i]\boldsymbol{e}^{(m)}\right|^2 = \sigma_s^2\boldsymbol{w}^{(a,k)H}[i]\boldsymbol{G}_R^{(a)}[i]\boldsymbol{E}_1\boldsymbol{E}_1^H\boldsymbol{G}_R^{(a)H}[i]\boldsymbol{w}^{(a,k)}[i] \\
P_{\mathrm{ITI}}^{(a,k)}[i] &= \mathcal{E}\left\{\left|\boldsymbol{w}^{(a,k)H}[i]\boldsymbol{b}_4[i]\right|^2\right\} = \boldsymbol{w}^{(a,k)H}[i]\boldsymbol{R}_{b_4}^{(a)}[i]\boldsymbol{w}^{(a,k)}[i] \\
P_{\mathrm{noise}}^{(a,k)}[i] &= \mathcal{E}\left\{\left|\boldsymbol{w}^{(a,k)H}[i]\boldsymbol{\xi}[i]\right|^2\right\} = \sigma_\xi^2\boldsymbol{w}^{(a,k)H}[i]\boldsymbol{w}^{(a,k)}[i] \quad (26)
\end{aligned}$$

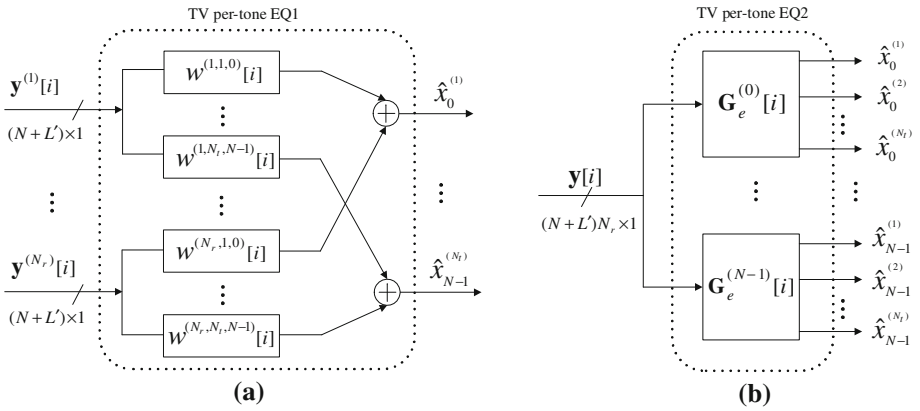

Fig. 3 Proposed time-domain per-tone equalizers, **a** Minimum BER method, **b** Minimum MSE method

where $\boldsymbol{e}^{(k)}$ is the $(k+1)$th unit vector of size $N \times 1$, $\boldsymbol{w}_k^{(a)}[i] = \boldsymbol{G}_R^{(a)}[i]\boldsymbol{E}_0\boldsymbol{e}^{(k)}$ and $\boldsymbol{R}_{b_4}^{(a)}[i] = \mathcal{E}\left\{\boldsymbol{b}_4[i]\boldsymbol{b}_4^H[i]\right\}$, where the (r_1, r_2)th element in this matrix is given by

$$[\boldsymbol{R}_{b_4}^{(a)}[i]]_{r_1,r_2} = \sigma_s^2 \sum_{\substack{t=1 \\ t\neq a}}^{N_t} \boldsymbol{G}^{(r_1,t)}[i]\boldsymbol{G}^{(r_2,t)H}[i] \tag{27}$$

Substituting (26) in (25), yields

$$\mathrm{SINR}^{(a,k)}[i] = \frac{\boldsymbol{w}^{(a,k)H}[i]\boldsymbol{w}_k^{(a)}[i]\boldsymbol{w}_k^{(a)H}[i]\boldsymbol{w}^{(a,k)}[i]}{\boldsymbol{w}^{(a,k)H}[i]\left(\boldsymbol{R}_k[i] + \frac{\sigma_\xi^2}{\sigma_s^2}\boldsymbol{I}_{N_r(N+L')}\right)\boldsymbol{w}^{(a,k)}[i]} \tag{28}$$

where $\boldsymbol{R}_k[i] = \boldsymbol{G}_R^{(a)}[i]\left(\boldsymbol{E}_0(\boldsymbol{I}_N - \boldsymbol{e}^{(k)}\boldsymbol{e}^{(k)T})\boldsymbol{E}_0^H + \boldsymbol{E}_{-1}\boldsymbol{E}_{-1}^H + \boldsymbol{E}_1\boldsymbol{E}_1^H\right)\boldsymbol{G}_R^{(a)H}[i] + \boldsymbol{R}_{b_4}^{(a)}[i]/\sigma_s^2$. Our aim is to design the time-domain equalizers $\{\boldsymbol{w}^{(a,k)}[i]\}_{k\in\mathcal{S}_u}$ such that the total BER in (20) can be minimized. However, note that the Q-function is always positive, so, it is sufficient to minimize the $\mathcal{P}_{\mathrm{bit}}^{(a,k)}[i]$ for all $k \in \mathcal{S}_u$. This means that we can design the equalizer $\boldsymbol{w}^{(a,k)}[i]$ for each subcarrier, separately. Also, the Q-function is monotonically decreasing. Hence, minimization of $\mathcal{P}_{\mathrm{bit}}^{(a,k)}[i]$ implies maximization of $\mathrm{SINR}^{(a,k)}[i]$. Therefore, the time-domain per-tone equalizer corresponding to the kth subcarrier of the ith OFDM block and the ath transmit transducer can be obtained by maximizing the $\mathrm{SINR}^{(a,k)}[i]$ in (28), which results in the following optimization problem

$$\begin{aligned} &\max_{\boldsymbol{w}^{(a,k)}[i]} \quad \boldsymbol{w}^{(a,k)H}[i]\boldsymbol{w}_k^{(a)}[i]\boldsymbol{w}_k^{(a)H}[i]\boldsymbol{w}^{(a,k)}[i] \\ &\text{subject to} \quad \boldsymbol{w}^{(a,k)H}[i]\left(\boldsymbol{R}_k[i] + \frac{\sigma_\xi^2}{\sigma_s^2}\boldsymbol{I}_{N_r(N+L')}\right)\boldsymbol{w}^{(a,k)}[i] = 1 \end{aligned} \tag{29}$$

This is a generalized eigenvalue problem whose solution is given by [25]

$$\boldsymbol{w}_{\mathrm{opt}}^{(a,k)}[i] = \left(\boldsymbol{G}_R^{(a)}[i]\boldsymbol{G}_R^{(a)H}[i] + \frac{\sigma_\xi^2}{\sigma_s^2}\boldsymbol{I}_{N_r(N+L')} + \frac{\boldsymbol{R}_{b_4}[i]}{\sigma_s^2}\right)^{-1}\boldsymbol{w}_k^{(a)}[i] \tag{30}$$

Figure 3a depicts the derived time-domain per-tone equalizer. The optimum SINR for the kth subcarrier of the ith OFDM block and the ath transmit transducer is obtained by substituting (30) in (28) which yields

$$\mathrm{SINR}_{\mathrm{opt}}^{(a,k)}[i] = \frac{\boldsymbol{w}_k^{(a)H}[i]\boldsymbol{w}_{\mathrm{opt}}^{(a,k)}[i]}{1 - \boldsymbol{w}_k^{(a)H}[i]\boldsymbol{w}_{\mathrm{opt}}^{(a,k)}[i]} \tag{31}$$

Finally, substituting (31) in (20) yields the minimum BER corresponding to the ith OFDM block and the ath transmit transducer.

4.2 MSE Minimization Method

The proposed per-tone equalization approach in Sect. 4.1, applies a separate equalizer for the kth subcarrier of each transmit transducer in the time domain. Here, we propose another time-domain per-tone equalization method which considers the kth subcarriers of all transmit transducers and equalizes them simultaneously (Fig. 3b). In other words, we use an equalizer matrix $\boldsymbol{G}_e^{(k)}[i]$ to estimate the N_t transmitted symbols on the kth subcarriers of the ith OFDM blocks at the N_t transmit transducers as

$$\hat{\boldsymbol{x}}_k[i] = \boldsymbol{G}_e^{(k)}[i]\boldsymbol{y}[i] \tag{32}$$

where $\hat{\boldsymbol{x}}_k[i]$ is an estimate of $\boldsymbol{x}_k[i] = [x_k^{(1)}[i], \ldots, x_k^{(N_t)}[i]]^T$. This equation shows that each transmitted symbol is estimated as a linear combination of the samples of the received signals. For each subcarrier, we can find the equalizer matrix $\boldsymbol{G}_e^{(k)}[i]$ by minimizing the following cost function

$$\mathcal{J}[i] = \mathcal{E}\left\{ \left\| \boldsymbol{x}_k[i] - \boldsymbol{G}_e^{(k)}[i]\boldsymbol{y}[i] \right\|^2 \right\} \tag{33}$$

Solving for $\boldsymbol{G}_e^{(k)}[i]$ in (33), we obtain

$$\boldsymbol{G}_{e,\,\mathrm{MMSE}}^{(k)}[i] = (\boldsymbol{I}_{N_t} \otimes \boldsymbol{e}^{(k)T})\boldsymbol{R}_x(\boldsymbol{G}[i]\mathbb{E}_0)^H(\boldsymbol{G}[i]\mathbb{E}_0\boldsymbol{R}_x(\boldsymbol{G}[i]\mathbb{E}_0)^H + \boldsymbol{R}_v)^{-1} \tag{34a}$$

$$= (\boldsymbol{I}_{N_t} \otimes \boldsymbol{e}^{(k)T})\left((\boldsymbol{G}[i]\mathbb{E}_0)^H\boldsymbol{R}_v^{-1}\boldsymbol{G}[i]\mathbb{E}_0 + \boldsymbol{R}_x^{-1}\right)^{-1}(\boldsymbol{G}[i]\mathbb{E}_0)^H\boldsymbol{R}_v^{-1} \tag{34b}$$

where (34b) is again obtained by using the matrix inversion lemma and $\boldsymbol{R}_x$ and $\boldsymbol{R}_v$ are defined in (14). For white input data and noise, this per-tone equalizer reduces to

$$\boldsymbol{G}_{e,\,\mathrm{MMSE}}^{(k)}[i] = (\boldsymbol{I}_{N_t} \otimes \boldsymbol{e}^{(k)T})\mathbb{E}_0{}^H\left(\boldsymbol{G}^H[i]\boldsymbol{G}[i] + \frac{\sigma_\xi^2}{\sigma_s^2}\boldsymbol{I}_{(3NN_t)}\right)^{-1}\boldsymbol{G}^H[i] \tag{35}$$

It can be proved that the time-domain per-tone equalizers proposed in this section are mathematically equivalent to the time-domain block equalizer proposed in Sect. 3 (see the "Appendix A"). Also, it can be shown that the proposed equalizers in Sects. 3 and 4 share a common mathematical framework based on the maximization of a generalized Rayleigh quotient. This framework unifies several earlier equalization methods for multicarrier transmission [26].

5 Complexity Analysis

In this section, we compare the complexities of our proposed equalization approaches. We denote the proposed time-domain block MMSE equalizer as Prop-TBEQ. We also denote the time-domain per-tone equalizers derived (in Sect. 4) based on BER and MSE minimization as Prop-TPEQ1 and Prop-TPEQ2, respectively. Two types of complexity are considered: design complexity and implementation complexity. The design complexity is the computational cost to design the equalizer. To design the Prop-TBEQ, we need a matrix inversion of size $(N_t N) \times (N_t N)$. This requires about $\mathcal{O}((N_t N)^3)$ flops per ith transmitted blocks of all transmit transducers. On the other hand, to design the Prop-TPEQ1, we require about $\mathcal{O}(N_r^3(N + L')^3)$ flops per ith transmitted blocks of all transmit transducers. So, the design complexity of Prop-TPEQ1 is greater than the design complexity of Prop-TBEQ. The design complexity of Prop-TPEQ2 is equal to the design complexity of Prop-TBEQ.

The implementation complexity is the computational cost to estimate the transmitted blocks once the equalizer has been designed. For the Prop-TBEQ, to estimate the ith block transmitted at the ath transmit transducer, we require $N_r N(N+L')$ multiply-add (MA) operations plus $\mathcal{O}(N \log_2 N)$ MA operations for the FFT. Whereas Prop-TPEQ1 and Prop-TPEQ2 require $N_r N(N+L')$ MA operations to estimate the ith block transmitted at the ath transmit transducer. So, the implementation complexity of the proposed per-tone equalizers is less than the implementation complexity of Prop-TBEQ.

6 Simulations

In this section, we provide simulation results to investigate the performance of the proposed equalization techniques in a typical shallow UWA channel.

6.1 Simulation Setup

We consider a single-input multiple-output (SIMO)–OFDM system with $N_r = 2$ receive transducers as well as a MIMO–OFDM system with $N_t = 2$ transmit transducers and $N_r = 4$ receive transducers. We assume that the receive (transmit) transducers are sufficiently spaced above the UWA channel coherence distance, so the received signals experience uncorrelated fading. Other parameters of the simulation are listed in Table 1.

Table 1 Simulation parameters

Parameter	Notation	Value
Doppler spread	$f_{\max}$	50 Hz
Delay spread	$\tau_{\max}$	2 ms
Sampling time	T	100 μs
Number of subcarriers	N	128
Cyclic prefix length	c	14
Channel order	L	20
Channel bandwidth	B	10 kHz
Decision delay	d	4
Discrete Doppler spread	$Q/2$	2

Recent experimental shallow UWA channel measurements used to examine several candidate fading models, indicate a good match with the Rician distribution [27]. Hence, we simulate the UWA channel as a Rician fading channel. We also consider the Rayleigh distribution as a special case of Rician fading. Underwater experiments have shown that typical shallow UWA channels have three prominent paths, namely the direct path, the bottom-reflected path, and the surface-reflected path [28]. In addition, the underwater channel impulse response is typically sparse, i.e., few propagation paths carry significant energy [29]. Thus, for testing the proposed equalizers, we consider four paths between each transmit and receive transducer pair. We simulate a "perfectly sparse" channel with $N_a = 4$ active taps or nonzero fading coefficients spread over $L = 20$ chip durations. The active taps are at path delays $\tau_0 = 0,\ \tau_1 = 0.4,\ \tau_2 = 1.1$, and $\tau_3 = 2\ msec$ and simulated using the model shown in Fig. 4. In this model, each tap is independently generated by passing a complex Gaussian random process with mean $\mu e^{j\varphi_{r,t}}$ and variance $2\sigma^2_{\text{Rice}}$ through an FIR fading filter with Gaussian-shaped power spectrum. The parameter $\varphi_{r,t}$ is the phase of the direct path between the tth transmit and the rth receive transducers. The normalized Gaussian Doppler power spectrum is given analytically by

$$S_G(f) = \left(1/\sqrt{\pi f^2_{\max}}\right) \exp\left(-f^2/f^2_{\max}\right) \tag{36}$$

where $f_{\max}$ is the channel maximum Doppler spread and $f_c = f_{\max}\sqrt{\ln 2}$ is the 3 dB cutoff frequency. Furthermore, we consider an exponential delay power profile (DPP), i.e. the lth tap power at delay τ_l is $\sigma_l^2 = c_0 \exp(-\tau_l/\tau_{\text{rms}})$, where τ_{rms} is the rms delay spread and c_0 is the normalization constant. We define the SNR as

$$\text{SNR} = \left((2\sigma^2_{\text{Rice}} + \mu^2) \sum_{\iota=0}^{L_f} \hbar_\iota^2 + \mu^2 \sum_{j=0}^{L_f} \sum_{\substack{\iota=0 \\ \iota \neq j}}^{L_f} \hbar_\iota \hbar_j \right) \sum_{l=0}^{N_a-1} c_0 \exp(-\tau_l/\tau_{\text{rms}}) \sigma_s^2/\sigma_\xi^2 \tag{37}$$

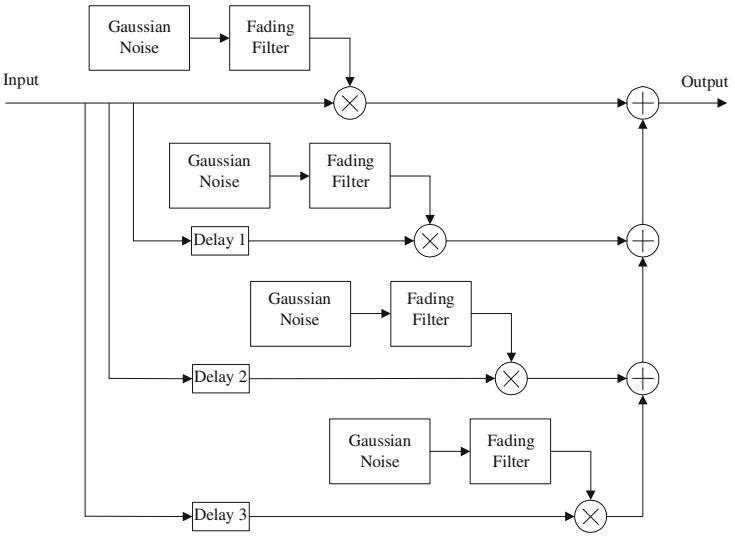

Fig. 4 Simulated model for shallow UWA channel

where $\hbar_\iota$ is the ιth tap gain of the normalized impulse response of the fading filter and L_f is the order of this filter.

We represent the simulated (true) channel by BEM. Then we obtain the BEM coefficients via least squares fitting of the simulated channel in the noiseless case. These coefficients are then used to design the equalizers for the true channel. In this paper, we only provide the simulation results for CE-BEM which is reasonably accurate and frequently used. However, our paper formulation is based on a general BEM, so simulation of the proposed equalization methods for other BEMs is straightforward. In CE-BEM, basis functions are complex exponential functions as $\psi_q(n) = e^{j2\pi qn/K}$, where K is the BEM frequency resolution [21]. The number of TV basis functions Q should satisfy $Q/(2KT) \geq f_{\max}$. Also we assume that the BEM frequency resolution K is an integer multiple of the FFT size, i.e. $K = PN$, where P is an integer greater than or equal to 1.

6.2 Simulation Results

First, we consider a SIMO-OFDM system with $N_r = 2$ receive transducers. Figure 5 compares the BER performances of the proposed block equalization approaches for Rayleigh and Rician fading channels when the BEM resolution is $K = 2N$. For Rician fading channel, the Rician factor $\mathcal{K}_R$ is defined as $\mathcal{K}_R = 10\log_{10}(\mu^2/(2\sigma^2_{\text{Rice}}))$ and is chosen to be $\mathcal{K}_R = 3\,\text{dB}$. As a benchmark, we consider the case of OFDM transmission over TI frequency selective channels where there is not any ICI or IBI. In this case, the one-tap MMSE equalizer is used that is an extension of the one-tap approach in [30] for SISO-OFDM (see the "Appendix B"). In addition, Fig. 5 illustrates the performance of the one-tap MMSE approach for doubly selective channel. As shown in this figure, the one-tap MMSE equalizer failed to compensate for the UWA channel distortion. However, proposed approaches provide significant inter-

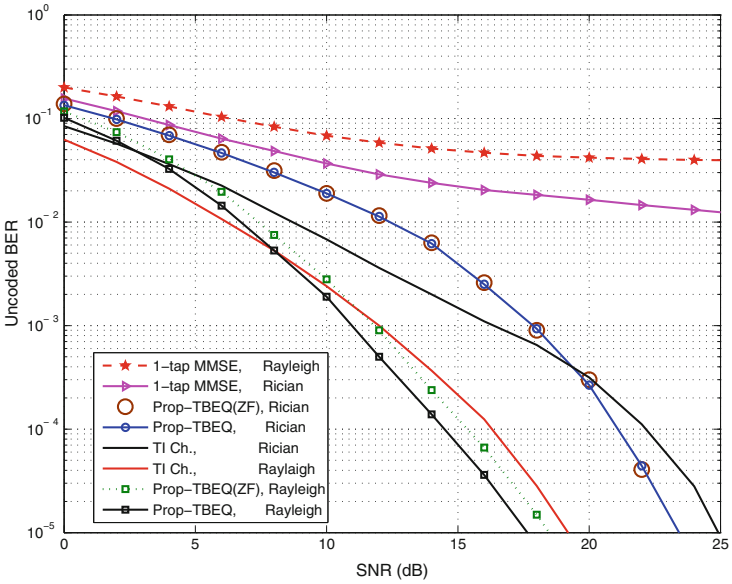

Fig. 5 BER comparison for SIMO-OFDM in Rayleigh and Rician channels, ($N_r = 2$, $\mathcal{K}_R = 3\,\text{dB}$)

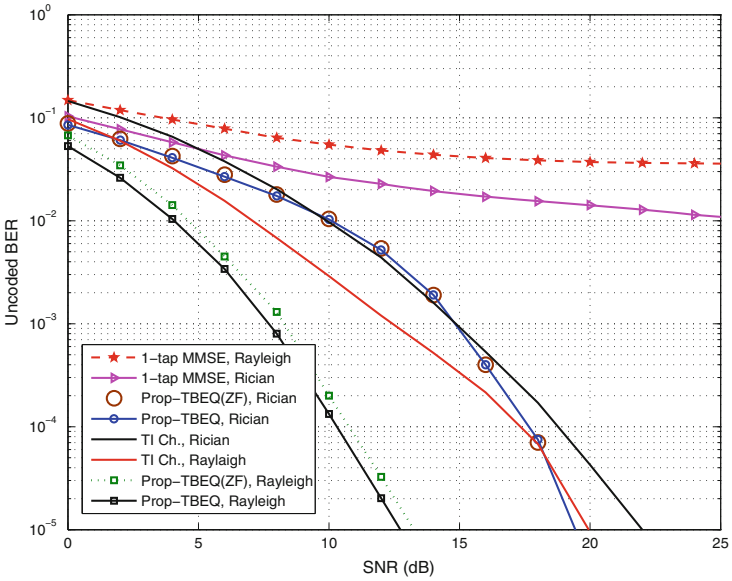

Fig. 6 BER comparison for MIMO–OFDM in Rayleigh and Rician channels ($N_t = 2,\ N_r = 4,\ \mathcal{K}_R = 3\,\text{dB}$)

ference cancellation. Furthermore, Prop-TBEQ outperforms the ZF equalizer in the case of Rayleigh fading channel.

Second, we consider a MIMO–OFDM system with $N_t = 2$ transmit transducers and $N_r = 4$ receive transducers to evaluate the performances of proposed equalizers for Rayleigh and Rician fading. The BEM resolution is chosen to be $K = 2N$ and the Rician factor is $\mathcal{K}_R = 3\,\text{dB}$. Figure 6 depicts the simulation results. Similar to the SIMO case, this figure illustrates that the one-tap MMSE approach failed to equalize the channel. It is also observed that the proposed methods considerably outperform the one-tap MMSE equalizer. Comparing Figs. 5 and 6 demonstrates the performance improvement when using MIMO transmission. It is seen that an average SNR gain of 3–5 dB is obtained for the MIMO case over the SIMO.

Third, we consider a SIMO-OFDM system with $N_r = 2$ receive transducers and examine the effect of BEM resolution (K) on the performance of equalization approaches in Rician fading channel when Rician factor ($\mathcal{K}_R$) changes. Figure 7 shows the BER performance of Prop-TPEQ1 for different values of Rician factor. As shown in this figure, for $\mathcal{K}_R = -30\,\text{dB}$, where the fading is nearly Rayleigh, choosing $K = N$ results in an early error floor at BER $= 1.4 \times 10^{-3}$ and SNR = 18 dB. In this case, increasing the BEM resolution to $K = 2N$, considerably improves the performance. Figure 7 shows that as the Rician factor becomes larger, the difference between BER curves corresponding to $K = N$ and $K = 2N$ decreases and the curves begin to get closer to each other. It is seen that for $\mathcal{K}_R = 10\,\text{dB}$, there is negligible difference between BER curves for $K = N$ and $K = 2N$. This simulation indicates that in Rician fading UWA channels, the BEM resolution has much less effect on the BER performance of Prop-TPEQ1 compared to Rayleigh fading channels. Other proposed equalizers show the same behavior.

Finally, we consider MIMO–OFDM transmission with $N_t = 2$ transmit transducers and $N_r = 4$ receive transducers to investigate the performance of Prop-TPEQ2 for a typical sparse channel. In the above simulations, we used a "perfectly sparse" channel. Here we

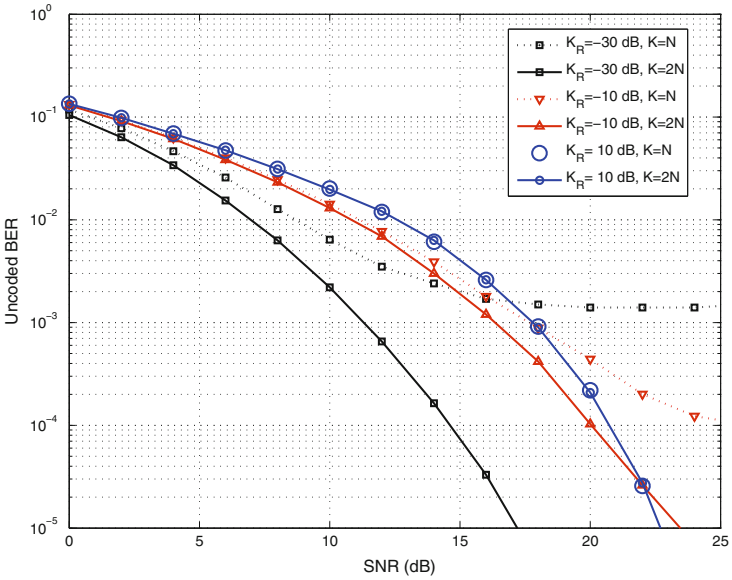

Fig. 7 BER versus SNR for different values of Rician factor $\mathcal{K}_R$ using per-tone BER minimizing equalizer (Prop-TPEQ1) in SIMO-OFDM system ($N_r = 2$)

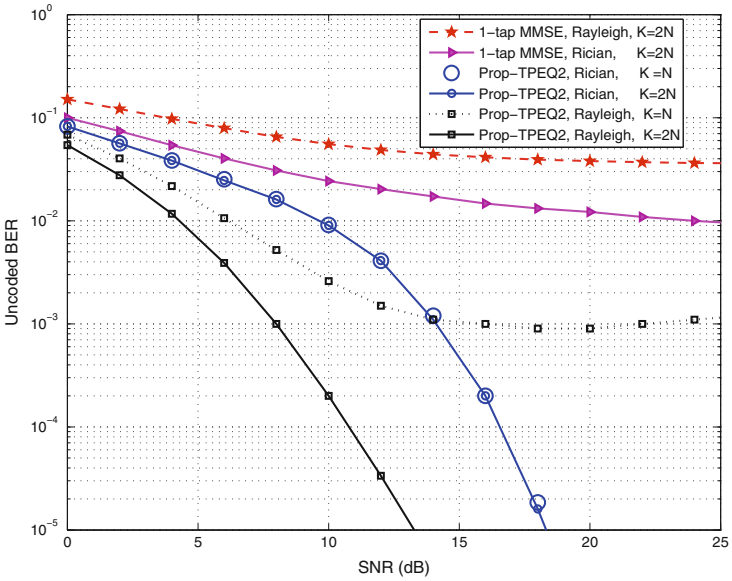

Fig. 8 BER versus SNR using per-tone MSE minimizing equalizer (Prop-TPEQ2) in a sparse channel for MIMO–OFDM system ($N_t = 2,\ N_r = 4,\ \mathcal{K}_R = 3\,\text{dB}$)

consider a more realistic "sparse" channel. To simulate this channel, 10 % of each active-tap energy is leaked into its neighboring inactive taps. The BER performance of Prop-TPEQ2 for different fading distributions and BEM resolutions is depicted in Fig. 8. For Rayleigh fading, when $K = N$, Prop-TPEQ2 significantly outperforms the one-tap MMSE. However, it suffers from an early error floor at BER $= 10^{-3}$ and SNR = 16 dB. One can observe that this

problem is resolved and the performance is significantly improved for $K = 2N$. For Rician fading (with $\mathcal{K}_R = 3\,\text{dB}$), in contrast to the Rayleigh fading case, the BER performance of Prop-TPEQ2 for different BEM resolutions ($K = N, 2N$) are almost the same and there is no early error floor.

7 Conclusion

In this paper, we addressed equalization of shallow underwater acoustic (UWA) channels when a MIMO–OFDM transmission system is used. We considered a general case where the channel delay spread is larger than the CP and the channel varies within each OFDM block. We proposed two time-domain block equalizers based on MMSE and ZF design criteria. We also proposed two time-domain per-tone equalization approaches, which optimize the performance on each subcarrier separately. The per-tone approaches were derived by minimizing the BER or MSE. A significant advantage of our proposed methods is that they need no redundancy or bandwidth expansion except for the CP. Moreover, it can be shown that the proposed equalizers fit into a unified framework for time-domain equalizers.

Our simulations showed that the proposed approaches considerably outperform the conventional one-tap MMSE equalizer. For UWA channels with Rayleigh fading distribution, increasing the BEM resolution beyond the size of the FFT (i.e., oversampling the received sequence in the frequency-domain), considerably improves the performance of proposed equalizers. However, for Rician distribution, our approaches are less sensitive to the BEM resolution. It is also observed that for large values of the Rician factor, increasing the BEM resolution does not improve the performance of proposed equalizers any more.

Appendix A: Equivalency of Proposed Equalizers

In this appendix, we prove that the proposed time-domain per-tone equalizers (Prop-TPEQ1 and Prop-TPEQ2) are mathematically equivalent to the proposed time-domain block equalizer (Prop-TBEQ). Based on (13a) and (17), the Prop-TBEQ uses the following matrix to estimate the transmitted blocks on all transmit transducers:

$$\bar{\boldsymbol{G}}_{e,\,\text{MMSE}}[i] = \boldsymbol{R}_x(\boldsymbol{G}[i]\mathbb{E}_0)^H \left(\boldsymbol{G}[i]\mathbb{E}_0\boldsymbol{R}_x(\boldsymbol{G}[i]\mathbb{E}_0)^H + \boldsymbol{R}_v\right)^{-1} \tag{38}$$

Substituting $\boldsymbol{R}_v$ from (14) in (38), the matrix $\bar{\boldsymbol{G}}_{e,\text{MMSE}}$ for white input data and noise reduces to

$$\bar{\boldsymbol{G}}_{e,\,\text{MMSE}}[i] = (\boldsymbol{G}[i]\mathbb{E}_0)^H \left(\boldsymbol{G}[i]\boldsymbol{G}^H[i] + \frac{\sigma_\xi^2}{\sigma_s^2}\boldsymbol{I}_{N_r(N+L')}\right)^{-1} \tag{39}$$

where we have used the equation $\mathbb{E}_0\mathbb{E}_0^H + \mathbb{E}_{-1}\mathbb{E}_{-1}^H + \mathbb{E}_1\mathbb{E}_1^H = \boldsymbol{I}_{(3N_tN)}$.

On the other hand, to estimate the transmitted symbol on the kth subcarrier of the ith OFDM block at the ath transmit transducer, we can use the Prop-TPEQ1 in (30) as

$$\boldsymbol{w}^{(a,k)}[i] = \left(\boldsymbol{G}_R^{(a)}[i]\boldsymbol{G}_R^{(a)H}[i] + \frac{\sigma_\xi^2}{\sigma_s^2}\boldsymbol{I}_{N_r(N+L')} + \frac{\boldsymbol{R}_{b_4}[i]}{\sigma_s^2}\right)^{-1} \boldsymbol{w}_k^{(a)}[i] \tag{40}$$

where $\boldsymbol{w}_k^{(a)}[i] = \boldsymbol{G}_R^{(a)}[i]\boldsymbol{E}_0\boldsymbol{e}^{(k)}$. We use (27) and $\boldsymbol{G}_R^{(a)}[i] = [\boldsymbol{G}^{(1,a)\,T}[i], \ldots, \boldsymbol{G}^{(N_r,a)\,T}[i]]^T$ to express $\boldsymbol{R}_{b_4}^{(a)}[i]$ in (40) as

$$\boldsymbol{R}_{b_4}^{(a)}[i] = \sigma_s^2 \sum_{\substack{t=1 \\ t\neq a}}^{N_t} \boldsymbol{G}_R^{(t)}[i]\boldsymbol{G}_R^{(t)H}[i]. \tag{41}$$

Substituting $\boldsymbol{R}_{b_4}^{(a)}[i]$ and $\boldsymbol{w}_k^{(a)}[i]$ in (40) and using the definitions for $\boldsymbol{G}_T^{(r)}[i]$, $\boldsymbol{G}[i]$ and $\boldsymbol{G}_R^{(a)}[i]$ in (5), (6) and (23) yields

$$\begin{aligned}\boldsymbol{w}^{(a,k)}[i] &= \left(\boldsymbol{G}_R^{(a)}[i]\boldsymbol{G}_R^{(a)H}[i] + \frac{\sigma_\xi^2}{\sigma_s^2}\boldsymbol{I}_{N_r(N+L')} + \sum_{\substack{t=1 \\ t\neq a}}^{N_t} \boldsymbol{G}_R^{(t)}[i]\boldsymbol{G}_R^{(t)H}[i]\right)^{-1} \boldsymbol{G}_R^{(a)}[i]\boldsymbol{E}_0\boldsymbol{e}^{(k)} \\ &= \left(\boldsymbol{G}[i]\boldsymbol{G}^H[i] + \frac{\sigma_\xi^2}{\sigma_s^2}\boldsymbol{I}_{N_r(N+L')}\right)^{-1} \boldsymbol{G}_R^{(a)}[i]\boldsymbol{E}_0\boldsymbol{e}^{(k)}\end{aligned} \tag{42}$$

In (42), only the term $\boldsymbol{e}^{(k)}$ depends on the subcarrier index k. Considering (42) for different subcarriers, we obtain

$$\boldsymbol{W}^{(a)}[i] = \left[\boldsymbol{w}^{(a,0)}[i], \ldots, \boldsymbol{w}^{(a,N-1)}[i]\right]^H = (\boldsymbol{G}_R^{(a)}[i]\boldsymbol{E}_0)^H \left(\boldsymbol{G}[i]\boldsymbol{G}^H[i] + \frac{\sigma_\xi^2}{\sigma_s^2}\boldsymbol{I}_{N_r(N+L')}\right)^{-1} \tag{43}$$

where $\boldsymbol{W}^{(a)}[i]$ contains the equalizers corresponding to all subcarriers of the ath transmit transducer.

Finally, the equalizer matrix used to recover the transmitted symbols on all subcarriers of all transmit transducers, based on the minimization of BER, is given by

$$\begin{aligned}\boldsymbol{W}_{\mathrm{BER}}[i] &= \left[\boldsymbol{W}^{(1)\,T}[i], \ldots, \boldsymbol{W}^{(N_t)\,T}[i]\right]^T \\ &= \left(\left[\boldsymbol{G}_R^{(1)}[i], \ldots, \boldsymbol{G}_R^{(N_t)}[i]\right](\boldsymbol{I}_{N_t} \otimes \boldsymbol{E}_0)\right)^H \left(\boldsymbol{G}[i]\boldsymbol{G}^H[i] + \frac{\sigma_\xi^2}{\sigma_s^2}\boldsymbol{I}_{N_r(N+L')}\right)^{-1}\end{aligned} \tag{44}$$

Using the definitions for $\boldsymbol{G}_T^{(r)}[i]$, $\boldsymbol{G}_R^{(a)}[i]$ and $\boldsymbol{G}[i]$, we can reduce (44) to

$$\boldsymbol{W}_{\mathrm{BER}}[i] = (\boldsymbol{G}[i]\mathbb{E}_0)^H \left(\boldsymbol{G}[i]\boldsymbol{G}^H[i] + \frac{\sigma_\xi^2}{\sigma_s^2}\boldsymbol{I}_{N_r(N+L')}\right)^{-1} \tag{45}$$

The equalizer matrices in (39) and (45) are the same. Therefore, the proposed BER minimizing equalizer (Prop-PTEQ1) is equivalent to the proposed block MMSE equalizer (Prop-BTEQ).

In addition, the proposed block MMSE equalizer uses the matrix $\bar{\boldsymbol{G}}_{e,\mathrm{MMSE}}[i]$ as in (38) to estimate the transmitted symbols on all subcarriers at all transmit transducers. To estimate the symbols corresponding to the kth subcarriers on all transmit transducers, we may use the corresponding N_t rows of the matrix$\bar{\boldsymbol{G}}_{e,\mathrm{MMSE}}[i]$ to obtain the following submatrix:

$$\bar{\boldsymbol{G}}_{e,\,\mathrm{MMSE}}^{(k)}[i] = (\boldsymbol{I}_{N_t} \otimes \boldsymbol{e}^{(k)T})\bar{\boldsymbol{G}}_{e,\,\mathrm{MMSE}}[i]$$
$$= (\boldsymbol{I}_{N_t} \otimes \boldsymbol{e}^{(k)T})\boldsymbol{R}_x(\boldsymbol{G}[i]\mathbb{E}_0)^H \left(\boldsymbol{G}[i]\mathbb{E}_0\boldsymbol{R}_x(\boldsymbol{G}[i]\mathbb{E}_0)^H + \boldsymbol{R}_v\right)^{-1} \tag{46}$$

Comparing the Eqs. (46) and (34a), we conclude that the per-tone MSE minimizing equalizer (Prop-PTEQ2) is also equivalent to the proposed block MMSE equalizer (Prop-BTEQ).

Appendix B: One-Tap MMSE Equalizer for MIMO–OFDM

In this appendix, we extend the one-tap MMSE equalizer proposed in [30] to MIMO–OFDM systems. Similar to (5), we express the received block of length N at the rth receive transducer as

$$\boldsymbol{y}'^{(r)}[i] = \sum_{t=1}^{N_t} \underbrace{\sum_{q=-Q/2}^{Q/2} \boldsymbol{\Psi}'_q[i]\left[\boldsymbol{O}'_1, \boldsymbol{H}'^{(r,t)}_q[i], \boldsymbol{O}'_2\right](\boldsymbol{I}_3 \otimes \boldsymbol{P})(\boldsymbol{I}_3 \otimes \boldsymbol{\mathcal{F}}^H)}_{\boldsymbol{G}'^{(r,t)}[i]} \underbrace{\begin{bmatrix}\boldsymbol{x}^{(t)}[i-1]\\ \boldsymbol{x}^{(t)}[i]\\ \boldsymbol{x}^{(t)}[i+1]\end{bmatrix}}_{\tilde{\boldsymbol{x}}^{(t)}} + \boldsymbol{\xi}'^{(r)}[i]$$
$$= \sum_{t=1}^{N_t} \boldsymbol{G}'^{(r,t)}[i]\tilde{\boldsymbol{x}}^{(t)} + \boldsymbol{\xi}'^{(r)}[i] = \boldsymbol{G}'^{(r)}_T[i]\tilde{\boldsymbol{x}} + \boldsymbol{\xi}'^{(r)}[i] \tag{47}$$

where $\boldsymbol{y}'^{(r)}[i] = [y^{(r)}[i(N+c)+c+d+1], \ldots, y^{(r)}[(i+1)(N+c)+d]]^T$, $\boldsymbol{\Psi}'_q[i] = \mathrm{diag}\{[\psi_q(i(N+c)+c+d+1), \ldots, \psi_q((i+1)(N+c)+d)]\}$, $\boldsymbol{O}'_1 = \boldsymbol{0}_{N\times(N+2c+d-L)}$, $\boldsymbol{O}'_2 = \boldsymbol{0}_{N\times(N+c-d)}$, $\boldsymbol{H}'^{(r,t)}_q[i]$ is an $N \times (N+L)$ Toeplitz matrix with the first column $[h^{(r,t)}_{q,L}[i], \boldsymbol{0}_{1\times(N-1)}]^T$ and the first row $[h^{(r,t)}_{q,L}[i], \ldots, h^{(r,t)}_{q,0}[i], \boldsymbol{0}_{1\times(N-1)}]$, $\boldsymbol{\xi}'^{(r)}[i] = [\xi'^{(r)}[i(N+c)+c+d+1], \ldots, \xi'^{(r)}[(i+1)(N+c)+d]]^T$, $\boldsymbol{G}'^{(r)}_T[i] = [\boldsymbol{G}'^{(r,1)}[i], \ldots, \boldsymbol{G}'^{(r,N_t)}[i]]$ and other parameters are defined as in (5).

Defining $\boldsymbol{y}'[i] = [\boldsymbol{y}'^{(1)T}[i], \ldots, \boldsymbol{y}'^{(N_r)T}[i]]^T$, $\boldsymbol{G}'[i] = [\boldsymbol{G}'^{(1)T}_T[i], \ldots, \boldsymbol{G}'^{(N_r)T}_T[i]]^T$ and $\boldsymbol{\xi}'[i] = [\boldsymbol{\xi}'^{(1)T}[i], \ldots, \boldsymbol{\xi}'^{(N_r)T}[i]]^T$, and using (47) we can express the received blocks (each of length N) at all receive transducers as

$$\boldsymbol{y}'[i] = \boldsymbol{G}'[i]\tilde{\boldsymbol{x}} + \boldsymbol{\xi}'[i] \tag{48}$$

We estimate the transmitted symbol on the kth subcarrier of the ith OFDM block at the ath transmit transducer as

$$\hat{x}^{(a)}_k[i] = \sum_{r=1}^{N_r} w^{(r,a,k)}[i]\boldsymbol{\mathcal{F}}^{(k)}\boldsymbol{y}'^{(r)}[i] = \boldsymbol{w}'^{(a,k)H}[i](\boldsymbol{I}_{N_r} \otimes \boldsymbol{\mathcal{F}}^{(k)})\boldsymbol{y}'[i] \tag{49}$$

where $\boldsymbol{w}'^{(a,k)}[i] = [w^{(1,a,k)}[i], \ldots, w^{(N_r,a,k)}[i]]^H$. To obtain the one-tap equalizer $\boldsymbol{w}'^{(a,k)}[i]$, we define the following MSE cost function

$$\mathcal{J}[i] = \mathcal{E}\left\{\left|x^{(a)}_k[i] - \boldsymbol{w}'^{(a,k)H}[i](\boldsymbol{I}_{N_r} \otimes \boldsymbol{\mathcal{F}}^{(k)})\boldsymbol{y}'[i]\right|^2\right\} \tag{50}$$

Hence, the MMSE coefficients for the kth subcarrier is obtained by solving $\partial \mathcal{J}[i]/\partial\, \boldsymbol{w}'^{(a,k)}[i] = 0$ which reduces to

$$\boldsymbol{w}'^{(a,k)}_{\mathrm{MMSE}}[i] = \Big((\boldsymbol{I}_{N_r} \otimes \boldsymbol{\mathcal{F}}^{(k)})(\boldsymbol{G}'[i]\boldsymbol{R}_{\tilde{x}}\boldsymbol{G}'^{H}[i] + \boldsymbol{R}_{\xi'})(\boldsymbol{I}_{N_r} \otimes \boldsymbol{\mathcal{F}}^{(k)H})\Big)^{-1} \times (\boldsymbol{I}_{N_r} \otimes \boldsymbol{\mathcal{F}}^{(k)})\boldsymbol{G}'[i]\boldsymbol{R}_{\tilde{x}}\boldsymbol{e}'^{(k)} \tag{51}$$

where $\boldsymbol{R}_{\tilde{x}} = \mathcal{E}\left\{\tilde{\boldsymbol{x}}[i]\tilde{\boldsymbol{x}}^{H}[i]\right\}$, $\boldsymbol{R}_{\xi'} = \mathcal{E}\left\{\boldsymbol{\xi}'[i]\boldsymbol{\xi}'^{H}[i]\right\}$, and $\boldsymbol{e}'^{(k)}$ is a $(3N_tN) \times 1$ unit vector with a 1 in the position $3N(a-1) + N + k + 1$.

References

1. Kilfoyle, D., & Baggeroer, A. (2000). The state of the art in underwater acoustic telemetry. *IEEE Journal of Oceanic Engineering, 25*(1), 4–27.
2. Chitre, M., Shahabudeen, S., & Stojanovic, M. (2008). Underwater acoustic communications and networking: Recent advances and future challenges. *Marine Technology Society Journal, 42*(1), 103–116.
3. Catipovic, J., Baggeroer, A., VonDer Heydt, K., & Koelsch, D. (1984). Design and performance analysis of a digital acoustic telemetry system for the short range underwater channel. *IEEE Journal of Oceanic Engineering, 9*(4), 242–252.
4. Stojanovic, M., Catipovic, J., & Proakis, J. G. (1993). Adaptive multichannel combining and equalization for underwater acoustic communications. *Journal of Acoustical Socity of America, 94*(3), 1621–1631.
5. Lam, W. K., & Ormondroyd, R. F. (1997). A coherent COFDM modulation system for a time-varying frequency-selective underwater acoustic channel. In: *Proceedings of international conference on electronic engineering in oceanography*, Southampton, UK, pp. 198–203
6. Kim, B.-Ch., & Lu, I.-T. (2000). Parameter study of OFDM underwater communuications system. In: *Proceedings of MTS/IEEE oceans conference*, Providence, USA, pp. 1251–1255
7. Frassati, F., Lafon, C., Laurent, P.-A., & Passerieux, J.-M. (2005). Experimental assessment of OFDM and DSSS modulations for use in littoral. In: *Proceedings of IEEE oceans conference*, Washington, D.C., USA, pp. 826–831
8. Zhang, Y., Sun, H., Cheng E., & Shen, W. (2010). An underwater acoustic implementation of DFT-spread OFDM. *EURASIP Journal of Advances in Signal Processing,* Article ID 572453, 6 pp.
9. LeBlanc, L. R., & Beaujean, P.-P. J. (2000). Spatio-temporal processing of coherent acoustic communication data in shallow water. *IEEE Journal of Oceanic Engineering, 25*(1), 40–51.
10. Roy, S., Duman, T. M., & McDonald, V. (2009). Error rate improvement in underwater MIMO communications using sparse partial response equalization. *IEEE Journal of Oceanic Engineering, 34*(2), 181–201.
11. Li, B., Zhou, Sh., Stojanovic, M., Freitag, L., Jie, H., & Willett, P. (2007). MIMO–OFDM over an underwater acoustic channel. In: *Proceedings of IEEE Oceans Conference*, Vancouver, Canada, pp. 1–6
12. Emre, Y., Kandasamy, V., Duman, T. M., Hursky, P., & Roy, S. (2008). Multi-input multi-output OFDM for shallow-water UWA communications. In: *Proceedings of acoustic conference*, Paris, France, pp. 5333–5338
13. Ma, X., Zhao, Ch., & Qiao, G. (2009). The underwater acoustic MIMO–OFDM system channel equalizer basing on independent component analysis. In: *Proceedings of WRI international conference on communication and mobile computing*, Kunming, Yunnan, pp. 568–572.
14. Ceballos Carrascosa, P., & Stojanovic, M. (2010). Adaptive channel estimation and data detection for underwater acoustic MIMO–OFDM systems. *IEEE Journal of Oceanic Engineering, 35*(3), 635–646.
15. Nisar, M. D., Utschick, W., Nottensteiner H., & Hindelang, T. (2007). On channel estimation and equalization of OFDM systems with insufficient cyclic prefix. In: *Proceedings of IEEE vehicular technology conference*, Dublin, pp. 1445–1449.
16. Hsu, C.-Y., & Wu, W.-R. (2009). Low-complexity ICI mitigation methods for high-mobility SISO/MIMO–OFDM systems. *IEEE Transactions on Vehicular Technology, 58*(6), 2755–2768.
17. Beheshti, M., Omidi, M. J., & Doost-Hoseini, A. M. (2009). Equalization of SIMO-OFDM systems with insufficient cyclic prefix in doubly selective channels. *IET Communications, 3*(12), 1870–1882.
18. Zemen, T., & Mecklenbräuker, F. (2005). Time-variant channel estimation using discrete prolate spheroidal sequences. *IEEE Transactions on Signal Processing, 53*(9), 3597–3607.

19. Hijazi, H., & Ros, L. (2009). Polynomial estimation of time-varying multipath gains with intercarrier interference mitigation in OFDM systems. *IEEE Transactions on Vehicular Technology, 58*(1), 140–151.
20. Teo, K. A. D., & Ohno, S. (2005). Optimal MMSE finite parameter model for doubly-selective channels. In: *Proceedings of IEEE global telecommunication conference*, St. Louis, MO, pp. 3503–3507
21. Giannakis, G. B., & Tepedelenlioğlu, C. (1998). Basis expansion models and diversity techniques for blind identification and equalization of time-varying channels. *Proceedings of IEEE, 86*(10), 1969–1986.
22. Barhumi, I., Leus, G., & Moonen, M. (2004). Per-tone equalization for OFDM over doubly selective channels. In: *Proceedings of IEEE international conference on communication*, Paris, France, pp. 2642–2647
23. Klein, A., Kaleh, G. K., & Baier, P. W. (1996). Zero forcing and minimum mean-square-error equalization for multiuser detection in code-division multiple-access channels. *IEEE Transactions on Vehicular Technology, 45*(2), 276–287.
24. Stuber, G. L. (2001). *Principles of mobile communications*. Norwell, MA: Kluwer.
25. Stamoulis, A., Diggavi, S. N., & Al-Dhahir, N. (2002). Intercarrier interference in MIMO–OFDM. *IEEE Transactions on Signal Processing, 50*(10), 2451–2464.
26. Martin, R. K., Vanbleu, K., Ding, M., Ysebaert, G., Milosevic, M., Evans, B. L., Moonen, M., & , Jr.Johnson, C. R. (2005). Unification and evaluation of equalization structures and design algorithms for discrete multitone modulation systems. *IEEE Transactions on Signal Processing, 53*(10), 3880–3894.
27. Radosevic, A., Proakis, J. G., & Stojanovic, M. (2009). Statistical characterization and capacity of shallow water acoustic channels. In: *Proceedings of IEEE oceans conference*, Bremen, Germany, pp. 1–8.
28. Bjem-Niese, C., Bjorno, L., Pinto, M. A., & Quellec, B. (1996). A simulation tool for high data-rate acoustic communication in a shallow-water time-varying channel. *IEEE Journal of Oceanic Engineering, 21*(2), 143–149.
29. Singer, A. C., Nelson, J. K., & Kozat, S. S. (2009). Signal processing for underwater acoustic communications. *IEEE Communication Magazine, 47*(1), 90–96.
30. Wang, Z., & Giannakis, G. B. (2000). Wireless multicarrier communications: Where Fourier meets Shannon. *IEEE Signal Processing Magazine, 17*(3), 29–48.

Author Biographies

Mojtaba Beheshti received the B.Sc. degree from the Isfahan University of Technology (IUT), Iran, the M.Sc degree from the University of Tehran, and the Ph.D. degree from IUT in 1996, 1999, and 2011 respectively, all in electrical engineering. From 2001-2004, he worked as a researcher in the Electrical & Computer Engineering research center of IUT. Currently he is an assistant professor with the Information and Communication Technology Institute of IUT. His research interests include: signal processing for digital communications, multicarrier and MIMO systems and underwater acoustic communications.

Mohammad Javad Omidi received his Ph.D. from University of Toronto in 1998. He worked in industry by joining a research and development group designing broadband communication systems for 5 years. In 2003 he joined the Department of Electrical and Computer Engineering, at Isfahan University of Technology, Iran; and then served as the chair of Information Technology Center and ECE department at this university. His research interests are in the areas of mobile computing, wireless communications, digital communication systems, cognitive radio, and VLSI architectures for communication algorithms.

Ali Mohammad Doost Hoseini received a B.Sc. degree in electrical engineering from Shiraz University, Iran, in 1975. M.Sc. and Ph.D. degrees were conferred to him, in the same field, by the University of California at Berkeley and Stanford University in 1978 and 1982, respectively. He joined Isfahan University of Technology in 1983 where he is currently an associate professor in the Electrical and Computer Engineering Department. He has taught numerous undergraduate and graduate courses in EE, and supervised several M.Sc. and Ph.D. dissertations, mainly, in the fields of estimation and digital communications.